Identifications of extreme ultraviolet spectra of Br-like to Ni-like neodymium ions using an electron beam ion trap

C Suzuki[1], Dipti[2], Y Yang[3], A Gall[3,4], R Silwal[3,5], S Sanders[3], A Naing[2], J Tan[2], E Takacs[2,3], Yu Ralchenko[2]

[1] National Institute for Fusion Science, 322-6 Oroshi-cho, Toki 509-5292, Japan
[2] National Institute of Standards and Technology, Gaithersburg, MD 20899, USA
[3] Department of Physics and Astronomy, Clemson University, Clemson, SC 29634, USA
[4] Harvard-Smithsonian Center for Astrophysics, 60 Garden Street, Cambridge, MA 02138, USA
[5] TRIUMF, Vancouver, BC V6T2A3, Canada

E-mail: csuzuki@nifs.ac.jp

Abstract. Accurate extreme ultraviolet spectra of open N-shell neodymium (Nd) ions were recorded at the electron beam ion trap facility of the National Institute of Standards and Technology. The measurements were performed for nominal electron beam energies in the range of 0.90 keV to 2.31 keV. The measured spectra were then compared with the spectra simulated by a collisional-radiative model utilizing atomic data produced with a fully relativistic atomic structure code. Consequently, 59 lines from Br-like to Ni-like Nd ions were unambiguously identified, most of which were newly assigned in this study. The wavelengths of 9 known lines from Ni-, Cu- and Zn-like Nd ions were in excellent agreement with previous measurements.

Keywords: highly charged ions, neodymium, EBIT, EUV spectra, collisional-radiative modelling

Submitted to: *J. Phys. B: At. Mol. Phys.*

1. Introduction

Identifications and compilations of extreme ultraviolet (EUV) and soft x-ray spectral lines emitted from lanthanides (Z=57–71) are less advanced compared to other elements due to limited experimental data and the complexities of their spectral structure. The allowed resonance transitions of highly charged lanthanide ions with electron configurations of [Ar]$3d^{10}4s^m$ (m=0–2) or [Ar]$3d^{10}4s^24p^m$ (m=1–6) mainly emit photons in the EUV and soft x-ray regions. This nature will possibly lead to applications of laser-produced plasmas of lanthanide elements to industrial short-wavelength light

sources [1, 2]. Recent progress of spectral analyses of soft x-ray emissions from laser-produced lanthanide plasmas have been reported in several papers [3–5]. However, experimental data on the spectral line identifications in these isoelectronic sequences are still limited to a few elements or ions with simple electron configurations and hence are insufficient for validating atomic theories of various lanthanide elements.

Electron beam ion traps (EBITs) can selectively generate ions with specific charge states of any injectable element by tuning the electron beam energy. Accordingly, EBITs are particularly helpful for systematic line identifications of highly charged ions of high Z elements, such as lanthanides. The EBIT facility at the National Institute of Standards and Technology (NIST) has been actively used for EUV investigations of samarium (Sm), dysprosium (Dy), erbium (Er), and ytterbium (Yb) ions [6–8]. Additional EUV studies of gadolinium (Gd) ions have also been carried out at NIST and Tokyo-EBIT facilities to serve the line identification needs of next generation light sources for EUV lithography [9, 10]. Complementing these experimental investigations of lanthanide elements, we focus on the EUV spectra from highly charged ions of neodymium (Nd, Z=60) having an unfilled outermost N-shell (n=4 orbitals). While low-charged Nd ions are often of astrophysical interest [11], studies of highly charged Nd ions are rather fundamental. Nevertheless, they can contribute to validations of atomic models for the other lanthanide elements relevant to industrial applications in terms of Z dependence.

The experimental identifications of Kr-like ([Ar]$3d^{10}4s^24p^6$) to Ni-like ([Ar]$3d^{10}$) Nd ions are currently limited to a few lines from charge states with simple electron configurations. In the early 1980s, a few isolated spectral lines of Cu- and Zn-like Nd ions were identified using high energy laser-produced plasmas [12–14]. Subsequently, the most prominent resonance and intercombination lines of Cu-, Zn- and Kr-like Nd ions have been identified in medium-sized tokamaks such as the Princeton Large Tokamak (PLT) [15, 16] and the Texas Experimental Tokamak (TEXT) [17, 18]. Later, Daido et al. reported soft X-ray lasing line from Ni-like Nd ions in a laser-produced plasma [19]. More recently, Suzuki et al. have made the assignment of another Ni-like Nd line of a magnetically confined torus plasma [20, 21]. However, spectral lines of other N-shell isoelectronic sequences have not yet been explored, and to our knowledge, there have been no EBIT data reported for Nd ions. As the continuation of our series of studies on lanthanides [6–9], we report the first systematic line identification of N-shell Nd ions produced with an EBIT to fill in this gap.

2. Experiment

The measurements were carried out at the NIST EBIT facility in Gaitherburg, MD, USA. The NIST EBIT has been described in great detail in previous works [6–9, 22], thus only a brief overview is given here. Neodymium ions, generated by a metal vapor vacuum arc (MeVVA) [23] ion source, are introduced into the trap region of the EBIT, where the ions are confined in the axial direction electrostatically and in the radial direction by the combination of electron beam space charge and an axial magnetic field

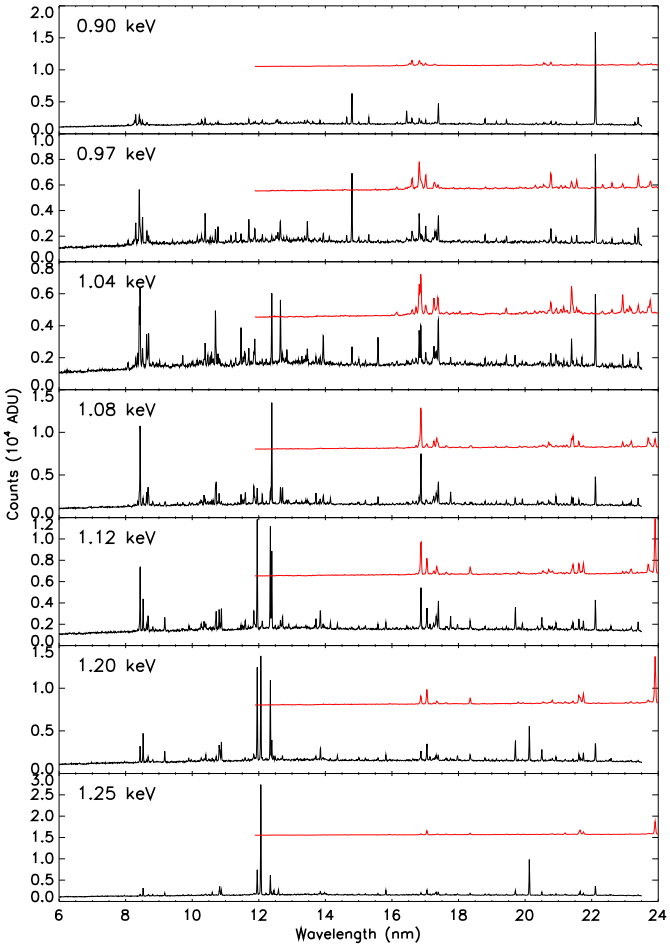

Figure 1: Measured EUV spectra (in analog-to-digital units (ADU) of the CCD detector) of Nd ions for nominal beam energies 0.90 keV–1.25 keV. The contributions of the second order spectra are shown by vertically shifted red lines.

of 2.7 T generated by a superconducting magnet surrounding the trap region. The quasi-monoenergetic electron beam is compressed by the magnetic field in the trap region that consists of three (upper, middle and lower) drift tube electrodes surrounded by a shield electrode. The voltages were kept at 220 V, 0 V, and 500 V for the upper, middle, and lower drift tubes, respectively, with respect to the shield voltage. The electron beam energy was controlled by tuning the shield voltage that determines the nominal beam energy. The experiment was performed with the beam energies in the range of 0.90 keV to 2.31 keV to produce the N-shell Nd ions. Note that the actual beam energy is estimated to be somewhat lower than the nominal beam energy due to the space charge of the electron beam. The beam current for the present experiment was in the range of 16 mA to 82.5 mA depending on the beam energy.

The EUV spectra of the emission from the trap region were measured by a grazing incidence spectrometer [24] equipped with a flat-field variable line-spacing grating with

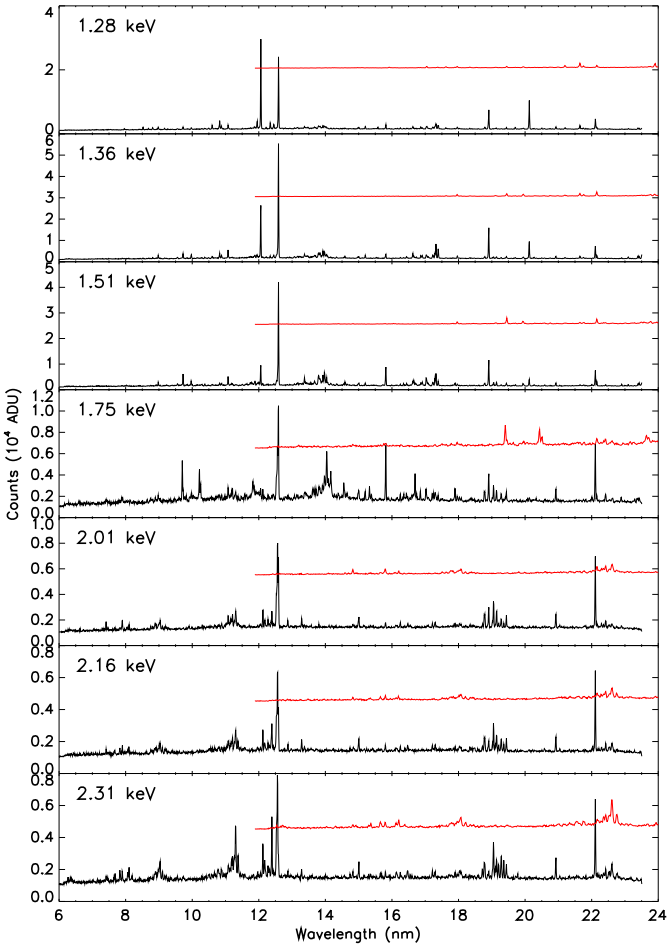

Figure 2: Measured EUV spectra (in analog-to-digital units (ADU) of the CCD detector) of Nd ions for nominal beam energies 1.28 keV–2.31 keV. The contributions of the second order spectra are shown by vertically shifted red lines.

a groove density of approximately 1200 mm^{-1}. The diffracted spectral image along the focal plane was recorded with a liquid nitrogen cooled back-illuminated charge coupled device (CCD) camera of 2048×512 pixels. In this study the wavelength coverage of the spectrometer was 6 nm to 23.5 nm with a resolving power of about 400. The observations of the EBIT plasma were taken with one-minute exposures, repeated ten times for each beam energy to automatically filter counts due to cosmic rays by removing outliers among different frames of an image of the same set. The absolute wavelength was calibrated using the well known lines of neon and iron ions, as well as ions of intrinsic impurities such as xenon, oxygen, argon, and barium. In the calibration procedure, a relation between the pixel and the wavelength of the selected reference lines was fitted by a third order polynomial, and the calibration and systematic uncertainties at each wavelength were determined by the procedure described in a previous article [7].

The measured EUV spectra in the nominal beam energy range of 0.90 keV to 2.31

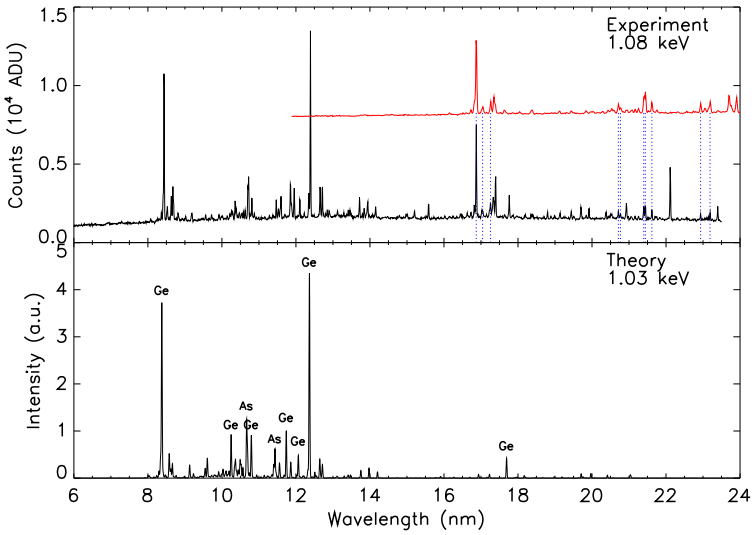

Figure 3: The measured and simulated EUV spectra of Nd ions for nominal beam energy of 1.08 keV. The contributions of the second order spectra are shown by vertically shifted red lines and vertical blue dotted lines in the measured spectrum. Some of the prominent lines are marked by their isoelectronic sequences in the theoretical spectrum.

keV are shown in Figs. 1 and 2. The measured spectra include lines from intrinsic impurities, e.g., Ar^{15+} at 22.115 nm. The plots of doubled wavelengths are superposed in red and shifted vertically to qualitatively represent the lines that originate from the second order spectra (see also vertical blue dotted lines in Figs. 3 and 4). For example, Fig. 1 reveals that for nominal beam energies below 1.1 keV, most of the lines observed in the wavelength region longer than 16 nm are second-order lines and lines from intrinsic impurities.

We normalized each experimental spectrum to the corresponding beam current and collection time, then each peak was fitted with a Gaussian profile to determine its intensity and wavelength with their statistical uncertainties. In the usual fitting procedure, we employed a formula including four free parameters (background, amplitude, center wavelength and linewidth). Though the linewidth in this experiment is dominated by instrumental width, we leave it free in the fitting procedure as it can fluctuate due to a slight change in experimental conditions. If required, a multi-Gaussian fitting was applied to separate partially blended lines as described in Section 4. The electron beam energy dependence of the line intensities was also used to help the line identification.

3. Comparison with collisional-radiative modeling

To aid in line identifications, the measured EUV spectra were compared with theoretical spectra simulated using the non-Maxwellian collisional-radiative (CR) modeling code NOMAD [25]. This procedure follows what has been successfully adopted in the previous

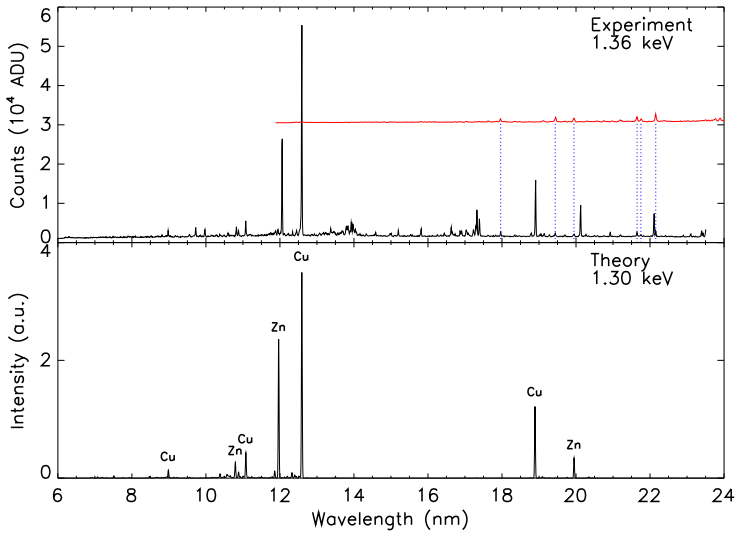

Figure 4: The measured and simulated EUV spectra of Nd ions for nominal beam energy of 1.36 keV. The contributions of the second order spectra are shown by vertically shifted red lines and vertical blue dotted lines in the measured spectrum. Some of the prominent lines are marked by their isoelectronic sequences in the theoretical spectrum.

studies of other lanthanide elements [6–9]. Atomic data necessary for the CR modeling were generated by the fully relativistic Flexible Atomic Code (FAC) [26]. Numerical data for radiative and collisional cross sections as well as energy level structures were calculated for Nd ions with the FAC code including singly excited configurations with a principal quantum number n up to 6–8 depending on the ion charge and doubly excited electron configurations within n=4 shell. Energies of the lowest n=4 levels were updated by another FAC calculation including all possible configurations within n=4 complex to improve the accuracy of the calculated wavelengths.

Using these atomic data, the steady-state rate equations were then solved using the NOMAD code [25]. Based on the recent studies [27, 28], the EBIT electron energy distribution function was assumed to be a 40-eV-wide Gaussian function around a specific electron beam energy. The ion stages included in the simulation were from Kr-like Nd^{24+} to Fe-like Nd^{34+} to cover the experimental beam energy range in this study. At every beam energy there were typically 3 to 5 ion charge states present in the trap. The electron density was set to be 10^{11} cm^{-3} in the present simulation. The calculated narrow spectral lines were convolved with the instrumental width and the intensities were adjusted by the spectral efficiency function of the spectrometer. The simulated spectra were generated with variable energy steps in the range of 20–100 eV.

Two examples of comparisons between the experiment and the simulation are shown in Figs. 3 and 4 for the nominal experimental beam energies of 1.08 keV and 1.36 keV, respectively, to demonstrate the validity of the simulation. The theoretical electron beam energy, selected based on the qualitative best match of theoretical and

experimental spectra, is lower than the experimental beam energy due to the space charge effect mentioned in Section 2. In Fig. 3, for example, the experimental spectrum taken at 1.08 keV qualitatively matches best with the simulation at 1.03 keV. The dominant ion stages at the nominal beam energies of 1.08 keV and 1.36 keV were Ge-like Nd^{28+} and Cu-like Nd^{31+}, respectively, as indicated in the bottom panels of Figs. 3 and 4. The spectral features of the prominent lines are well reproduced by the simulation, though some unidentified structures, most likely due to impurities, are observed in Fig. 4 in the 13 nm–18 nm wavelength region. These comparisons suggest that the present simulations are appropriate to provide unique identifications of most of the measured spectral lines.

Table 1: List of identified lines of highly charged neodymium ions in this study. The first column shows the ion charge and isoelectronic sequences in brackets. The experimental (λ_{exp}) and theoretical ($\lambda_{\mathrm{theory}}$) wavelengths are listed in nm. The uncertainties in the last significant digits of the measured wavelengths are shown in parentheses. In the column 'Present (FAC)', the lower and upper levels of a transition are shown in square brackets by using numbers designated consecutively from #1 (ground state) in order of energy. The previous theoretical wavelengths (the last column) in parentheses are derived from semi-empirical prediction.

	Lower level		Upper level		λ_{exp} (nm)		$\lambda_{\mathrm{theory}}$ (nm)	
Ion	Conf.	State	Conf.	State	Present	Previous	Present (FAC)	Previous
32+ [Ni]	$3d^9 4p$	$((3d^3_-)_{3/2}, 4p_-)_1$	$3d^9 4d$	$((3d^3_-)_{3/2}, 4d_-)_0$	7.4132(5)	7.413(2)[a]	7.0737 [9–35]	7.306[b]
						7.448[c]		
						(7.420[d])		
32+ [Ni]	$3d^9 4p$	$((3d^5_+)_{5/2}, 4p_+)_1$	$3d^9 4d$	$((3d^3_-)_{3/2}, 4d_-)_0$	7.8993(7)	7.903(2)[a]	7.5154 [12–35]	7.784[b]
						7.92(2)[c]		7.937[c]
						7.906(10)[e]		(7.905[d])
								(7.906[f])
31+ [Cu]	4p	$(4p_-)_{1/2}$	4d	$(4d_-)_{3/2}$	8.9788(6)	8.987(2)[a]	8.9849 [2–4]	8.984[g]
						8.9844(15)[h]		8.965[i]
								(8.9825[j])
								(8.9845[k])
31+ [Cu]	4d	$(4d_+)_{5/2}$	4f	$(4f_+)_{7/2}$	10.8803(8)*	10.8820(15)[h]	10.8840 [5–7]	10.91[i]
								(10.8836[j])
								(10.8820[k])
31+ [Cu]	4p	$(4p_+)_{3/2}$	4d	$(4d_+)_{5/2}$	11.0763(6)	11.0778(15)[h]	11.0792 [3–5]	11.04[i]
								(11.0780[j])
								(11.0778[k])
31+ [Cu]	4s	$(4s_+)_{1/2}$	4p	$(4p_+)_{3/2}$	12.5906(7)	12.5896(15)[h]	12.5920 [1–3]	12.57[i]

	Lower level		Upper level		$\lambda_{\rm exp}$(nm)		$\lambda_{\rm theory}$(nm)	
Ion	Conf.	State	Conf.	State	Present	Previous	Present (FAC)	Previous
						12.5920(5)[l]		(12.5911[j])
						12.592(3)[m]		(12.5897[k])
								12.593[n]
								12.593[o]
31+ [Cu]	4s	$(4s_+)_{1/2}$	4p	$(4p_-)_{1/2}$	18.9077(7)	18.9111(5)[l]	18.8925 [1–2]	18.82[i]
						18.904(3)[m]		(18.9095[j])
								(18.8968[k])
								18.913[n]
								18.914[o]
30+ [Zn]	4s4d	$(4s_+, 4d_+)_2$	4s4f	$(4s_+, 4f_+)_3$	10.5990(6)		10.5667 [14–30]	10.5493[p]
								(10.5728[q])
30+ [Zn]	4s4p	$(4s_+, 4p_+)_1$	4s4d	$(4s_+, 4d_+)_2$	10.8248(6)		10.7963 [5–14]	10.7762[p]
								(10.8275[q])
30+ [Zn]	$4s^2$	$(4s_+^2)_0$	4s4p	$(4s_+, 4p_+)_1$	12.0610(6)	12.0597(5)[l]	11.9659 [1–5]	11.9806[p]
						12.0589(10)[r]		(12.0614[q])
								12.0594[s]
								12.0644[t]
								12.0596[u]
								12.0640[v]
								12.0665[w]
								12.0500[x]
30+ [Zn]	4s4p	$(4s_+, 4p_-)_1$	$4p^2$	$(4p_-, 4p_+)_2$	12.4518(18)		12.4422 [3–8]	12.4199[p]
								(12.4380[q])
30+ [Zn]	$4s^2$	$(4s_+^2)_0$	4s4p	$(4s_+, 4p_-)_1$	20.1249(4)	20.1265(5)[l]	19.9475 [1–3]	20.1490[p]

	Lower level		Upper level		$\lambda_{\rm exp}$(nm)		$\lambda_{\rm theory}$(nm)	
Ion	Conf.	State	Conf.	State	Present	Previous	Present (FAC)	Previous
						20.13(1)[y]		(20.1261[q])
								20.1170[s]
								20.1344[t]
								20.1167[u]
								20.1313[v]
								20.1337[x]
29+ [Ga]	$4p$	$(4p_-)_{1/2}$	$4d$	$(4d_-)_{3/2}$	8.5256(3)		8.4737 [1–11]	8.471[z]
29+ [Ga]	$4p$	$(4p_-)_{1/2}$	$4s4p^2$	$(4s_+, (4p_+^2)_2)_{3/2}$	9.1761(4)*‡		9.1281 [1–10]	9.133[z]
29+ [Ga]	$4s4p^2$	$((4s_+, 4p_-)_1, 4p_+)_{3/2}$	$4s4p4d$	$((4s_+, 4p_-)_1, 4d_+)_{5/2}$	10.8094(4)*‡		10.7828 [6–23]	
29+ [Ga]	$4p$	$(4p_+)_{3/2}$	$4d$	$(4d_-)_{3/2}$	10.8753(9)*		10.7828 [2–11]	10.775[z]
29+ [Ga]	$4p$	$(4p_-)_{1/2}$	$4s4p^2$	$((4s_+, 4p_-)_1, 4p_+)_{1/2}$	11.9531(9)†		11.8586 [1–7]	11.867[z]
29+ [Ga]	$4p$	$(4p_+)_{3/2}$	$4s4p^2$	$(4s_+, (4p_+^2)_2)_{3/2}$	11.9531(9)†		11.8654 [2–10]	11.870[z]
29+ [Ga]	$4p$	$(4p_-)_{1/2}$	$4s4p^2$	$((4s_+, 4p_-)_1, 4p_+)_{3/2}$	12.3473(4)		12.3255 [1–6]	12.336[z]
29+ [Ga]	$4p$	$(4p_+)_{3/2}$	$4s4p^2$	$(4s_+, (4p_+^2)_2)_{5/2}$	13.8484(12)*		13.9043 [2–8]	13.919[z]
29+ [Ga]	$4p$	$(4p_-)_{1/2}$	$4s4p^2$	$((4s_+, 4p_-)_0, 4p_+)_{3/2}$	14.3626(12)		14.4520 [1–4]	14.469[z]
29+ [Ga]	$4p$	$(4p_+)_{3/2}$	$4s4p^2$	$((4s_+, 4p_-)_1, 4p_+)_{3/2}$	17.9683(10)*		17.9019 [2–6]	17.914[z]
29+ [Ga]	$4p$	$(4p_-)_{1/2}$	$4s4p^2$	$(4s_+)_{1/2}$	19.7073(5)*		19.7579 [1–3]	19.779[z]
29+ [Ga]	$4p$	$(4p_+)_{3/2}$	$4s4p^2$	$((4s_+, 4p_-)_1, 4p_+)_{5/2}$	20.5024(8)		20.5767 [2–5]	20.595[z]
29+ [Ga]	$4p$	$(4p_+)_{3/2}$	$4s4p^2$	$((4s_+, 4p_-)_0, 4p_+)_{3/2}$	22.5806(10)		22.7677 [2–4]	22.795[z]
28+ [Ge]	$4p^2$	$(4p_-^2)_0$	$4p4d$	$(4p_-, 4d_-)_1$	8.4352(3)		8.3754 [1–16]	
28+ [Ge]	$4p^2$	$(4p_-, 4p_+)_2$	$4p4d$	$(4p_+, 4d_-)_3$	8.6724(12)*§		8.6226 [3–23]	
28+ [Ge]	$4p^2$	$(4p_-^2)_0$	$4s4p^3$	$((4s_+, 4p_-)_1, (4p_+^2)_2)_1$	9.1849(9)*		9.1290 [1–13]	
28+ [Ge]	$4p^2$	$(4p_-, 4p_+)_2$	$4p4d$	$(4p_-, 4d_+)_3$	10.7205(8)*§		10.6917 [3–15]	

	Lower level		Upper level		$\lambda_{\rm exp}$(nm)		$\lambda_{\rm theory}$(nm)	
Ion	Conf.	State	Conf.	State	Present	Previous	Present (FAC)	Previous
28+ [Ge]	$4s4p^3$	$(4s_+,\ 4p_+)_1$	$4s4p^24d$	$(4s_+,\ 4d_+)_2$	10.8088(3)*‡		10.7952 [7–33]	
28+ [Ge]	$4p^2$	$(4p_-,\ 4p_+)_2$	4p4d	$(4p_-,\ 4d_-)_2$	11.5939(22)		11.5547 [3–14]	
28+ [Ge]	$4p^2$	$(4p_-,\ 4p_+)_2$	$4s4p^3$	$((4s_+,\ 4p_-)_1,\ (4p_+^2)_2)_1$	11.8512(5)		11.7389 [3–13]	
28+ [Ge]	$4p^2$	$(4p_-,\ 4p_+)_1$	$4s4p^3$	$((4s_+,\ 4p_-)_1,\ (4p_+^2)_0)_1$	12.1044(6)		12.0643 [2–12]	
28+ [Ge]	$4p^2$	$(4p_-^2)_0$	$4s4p^3$	$(4s_+,\ 4p_+)_1$	12.3903(3)		12.3644 [1–7]	
28+ [Ge]	$4p^2$	$(4p_-,\ 4p_+)_2$	4p4d	$(4p_-,\ 4d_-)_2$	12.7122(7)		12.7163 [3–11]	
28+ [Ge]	$4p^2$	$(4p_-,\ 4p_+)_2$	$4s4p^3$	$((4s_+,\ 4p_-)_1,\ (4p_+^2)_2)_3$	13.7173(11)		13.7546 [3–9]	
28+ [Ge]	$4p^2$	$(4p_-,\ 4p_+)_1$	$4s4p^3$	$((4s_+,\ 4p_-)_0,\ (4p_+^2)_2)_2$	14.1517(3)		14.2034 [2–8]	
28+ [Ge]	$4p^2$	$(4p_-,\ 4p_+)_2$	$4s4p^3$	$(4s_+,\ 4p_+)_1$	17.7625(3)		17.6919 [3–7]	
28+ [Ge]	$4p^2$	$(4p_-,\ 4p_+)_1$	$4s4p^3$	$(4s_+,\ 4p_+)_2$	19.9179(7)		19.9692 [2–6]	
28+ [Ge]	$4p^2$	$(4p_+^2)_2$	$4s4p^3$	$((4s_+,\ 4p_-)_1,\ (4p_+^2)_2)_3$	20.3769(16)		20.4157 [4–9]	
27+ [As]	$4p^3$	$(4p_+)_{3/2}$	$4p^24d$	$((4p_-,\ 4p_+)_2,\ 4d_+)_{3/2}$	8.3624(5)		8.3001 [1–25]	
27+ [As]	$4p^3$	$(4p_+)_{3/2}$	$4p^24d$	$((4p_-,\ 4p_+)_1,\ 4d_+)_{3/2}$	8.6328(3)		8.5761 [1–22]	
27+ [As]	$4p^3$	$(4p_+)_{3/2}$	$4p^24d$	$((4p_-,\ 4p_+)_1,\ 4d_+)_{5/2}$	8.6915(10)*§		8.6618 [1–21]	
27+ [As]	$4p^3$	$(4p_-,\ (4p_+^2)_2)_{3/2}$	$4p^24d$	$((4p_-,\ 4p_+)_2,\ 4d_+)_{5/2}$	9.7152(4)		9.6043 [2–28]	
27+ [As]	$4p^3$	$(4p_+)_{3/2}$	$4p^24d$	$(4d_+)_{5/2}$	10.6989(17)*§		10.6680 [1–10]	
27+ [As]	$4p^3$	$(4p_+)_{3/2}$	$4p^24d$	$(4d_-)_{3/2}$	11.4665(7)		11.4342 [1–9]	
27+ [As]	$4p^3$	$(4p_+)_{3/2}$	$4s4p^4$	$(4s_+,\ (4p_+^2)_2)_{3/2}$	12.6514(4)*		12.6445 [1–7]	
27+ [As]	$4p^3$	$(4p_+)_{3/2}$	$4s4p^4$	$(4s_+,\ (4p_+^2)_2)_{5/2}$	13.9368(11)		13.9752 [1–6]	
27+ [As]	$4p^3$	$(4p_-,\ (4p_+^2)_2)_{3/2}$	$4s4p^4$	$(4s_+,\ (4p_+^2)_2)_{5/2}$	19.6971(9)*		19.7072 [2–6]	
26+ [Se]	$4p^4$	$(4p_+^2)_2$	$4p^34d$	$((4p_-,\ (4p_+^2)_2)_{3/2},\ 4d_-)_3$	8.4102(8)		8.3346 [1–32]	8.286[aa]
26+ [Se]	$4p^4$	$(4p_+^2)_2$	$4p^34d$	$((4p_-,\ (4p_+^2)_0)_{1/2},\ 4d_+)_2$	8.5073(9)		8.4121 [1–31]	8.376[aa]
26+ [Se]	$4p^4$	$(4p_+^2)_2$	$4p^34d$	$(4p_+,\ 4d_+)_3$	10.3882(6)		10.3408 [1–14]	10.279[aa]

	Lower level		Upper level		$\lambda_{\rm exp}$(nm)		$\lambda_{\rm theory}$(nm)	
Ion	Conf.	State	Conf.	State	Present	Previous	Present (FAC)	Previous
26+ [Se]	$4p^4$	$(4p_+^2)_2$	$4p^34d$	$(4p_+, 4d_+)_2$	10.7752(7)		10.7392 [1–13]	10.702[aa]
26+ [Se]	$4p^4$	$(4p_+^2)_2$	$4p^34d$	$(4p_+, 4d_-)_1$	11.3072(3)		11.2618 [1–11]	11.230[aa]
26+ [Se]	$4p^4$	$(4p_+^2)_2$	$4p^34d$	$(4p_+, 4d_-)_3$	11.7016(5)		11.6774 [1–10]	11.627[aa]
26+ [Se]	$4p^4$	$(4p_+^2)_2$	$4s4p^5$	$(4s_+, (4p_+^3)_{3/2})_1$	12.6458(7)*		12.6325 [1–7]	12.648[aa]
26+ [Se]	$4p^4$	$(4p_+^2)_2$	$4s4p^5$	$(4s_+, (4p_+^3)_{3/2})_2$	13.4588(6)		13.4712 [1–6]	13.529[aa]
25+ [Br]	$4p^5$	$(4p_+^3)_{3/2}$	$4p^44d$	$((4p_-, (4p_+^3)_{3/2})_2\ 4d_-)_{5/2}$	8.3023(3)		8.2006 [1–27]	
25+ [Br]	$4p^5$	$(4p_+^3)_{3/2}$	$4p^44d$	$((4p_+^2)_2, 4d_+)_{5/2}$	10.2817(11)		10.2223 [1–14]	

* blended with another charge state or intrinsic impurity.

† blended with the same charge state.

‡ derived from the 2nd order spectrum.

§ derived from double-Gaussian fitting.

References: [a] [20]; [b] [30]; [c] [19]; [d] [31]; [e] [29]; [f] [32]; [g] [33]; [h] [13]; [i] [34]; [j] [35]; [k] [36]; [l] [17]; [m] [16]; [n] [37]; [o] [38]; [p] [39]; [q] [40]; [r] [14]; [s] [41]; [t] [42]; [u] [43]; [v] [44]; [w] [45]; [x] [46]; [y] [15]; [z] [47]; [aa] [48].

4. Identification results

The results of the present line identifications are summarized in Table 1 in which 59 lines from Ni-like Nd^{32+} to Br-like Nd^{25+} charge states are unambiguously assigned. If possible, the measured wavelengths and uncertainties listed in Table 1 are derived from weighted averages of fitting results at multiple beam energies. Questionable identifications due to complicated line blending or weak line intensities are excluded from Table 1. The isoelectronic sequences of the ion charge states are shown in brackets in the first column, followed by the configuration. The lower and upper levels of the transitions, denoted by jj coupling notation, were adopted from FAC. The present experimental wavelengths are listed together with those calculated with FAC followed by the numbers representing the upper and lower levels in the FAC calculations in brackets. The overall uncertainties in the last significant digits associated with the measured wavelengths are shown in parentheses in Table 1. As mentioned in Section 2, this overall uncertainty was evaluated as a combination of the calibration uncertainty, the fitting uncertainty, and the statistically determined systematic uncertainty. Note that some of the lines are blended with a line of another charge state or an intrinsic impurity, as indicated by footnotes in Table 1. Unambiguous assignments were possible by carefully analysing the electron beam-energy dependence of the intensity of the specific line.

Some of the lines of Ni-, Cu- and Zn-like ions have already been identified in previous experimental studies [13–17, 19, 20, 29]. These wavelengths are listed in Table 1 for reference. While majority of the theoretical studies have also focused on these charge states owing to their simple structure having one- or two- valence electrons in the outer shell [30–46], some atomic systems with multi-valence electrons, e.g., belonging to Ga-like and Se-like isoelectronic sequences, have been previously studied [47, 48]. These theoretical predictions are given in the last column of Table 1.

The excellent agreements seen between our measured wavelengths and the previous experiments strongly support the validity of our identifications for Ni-, Cu- and Zn-like Nd ions. Previously predicted wavelengths of the two transitions of Ni-like ions calculated by adjusting the *ab initio* energies by experimentally derived empirical constants are in very good agreement with our measured values [31]. Another calculation based on the relativistic multi-configuration Dirac-Fock approach also agree with the measured wavelengths [19]. The wavelengths calculated with the FAC package for these transitions of Ni-like ions showed a relatively larger discrepancy as compared to lines in the other charge stages. The ground configuration of Ni-like ion is a closed-shell $[Ar]3d^{10}$, whereas the ground configurations for the other charge states are $[Ar]3d^{10}4s^{m}$ (m=1–2) or $[Ar]3d^{10}4s^{2}4p^{m}$ (m=1–5). For Ni-like Nd^{32+} ion, the present FAC calculation was carried out considering single-electron excitation from $3l$ subshells (core) up to n=6. The limited core and valence shell correlations were included only for Ni-like, Cu-like, and Zn-like Nd ions, which can change the level energies. As an example, the inclusion of core-valence correlations in Cu-like ions changed the wavelength of resonance transition from 12.3970 nm to 12.5920 nm, where the latter value with increased correlations is

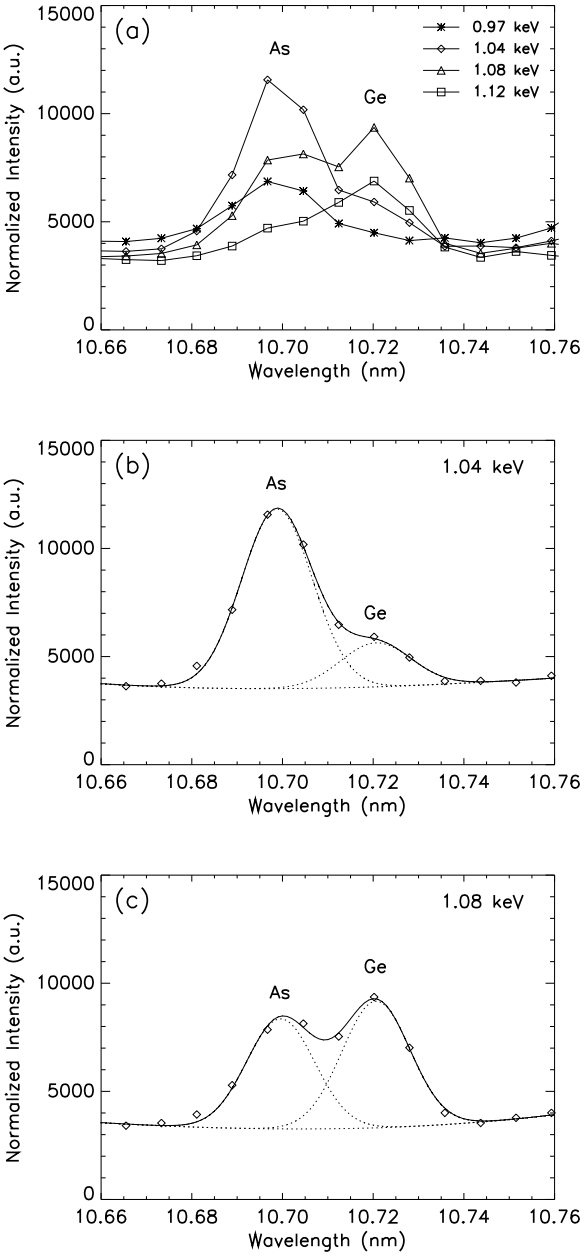

Figure 5: An example of the double-Gaussian fitting to identify partially blended lines of As-like Nd^{27+} at 10.6989 nm and Ge-like Nd^{28+} at 10.7205 nm. (a) An enlarged view of the spectra measured at 4 different nominal electron beam energies in the range of 0.97–1.12 keV. (b) The double-Gaussian fitting for the nominal electron beam energy of 1.04 keV. The experimental data (diamonds) are shown with the fit (solid line), which is the sum of two shifted Gaussian functions and a third-order polynomial function as a background (broken lines). (c) Similar plot for the nominal electron beam energy of 1.08 keV.

closer to the measured value 12.5906(7) nm. Electron correlation effects arising due to the interaction of doubly (or multi-) excited configurations from $3l$ subshells may be important for these two transitions of Ni-like ions [19], which were not included in our calculations.

The three lines of Zn-like ions at 10.5990 nm, 10.8248 nm, and 12.4518 nm have not been experimentally reported previously. For these lines, the wavelengths were predicted based on a semiempirical correction with the values of 10.5728 nm, 10.8275 nm, and 12.4380 nm, respectively [40].

Many lines of Ga-like to Br-like ions listed in Table 1 are identified for the first time in this study. Even in cases where a specific line is blended with a line of another charge state, identification is sometimes possible with the careful examination of the electron beam energy dependence of the spectral features as mentioned above. Due to the dense concentration of lines of these ion stages in the wavelength range shorter than approximately 13 nm, some of these assignments have been carried out by using double-Gaussian fitting to distinguish partially blended lines, as indicated by the footnote in Table 1. An example of the double-Gaussian fitting is shown in Fig. 5 for Ge- and As-like lines at 10.7205 nm and 10.6989 nm, respectively, where the vertical axis is converted to the normalized intensity. As demonstrated in Fig. 5, the measured experimental data were fitted well using the sum of two shifted Gaussian functions and a third-order polynomial function fit to the background. The line intensity ratio of these two lines changes for the nominal beam energies of 1.04 and 1.08 keV, following the expected beam energy dependence of these isoelectronic sequences.

For some cases, the present identifications can be validated by checking the agreements of the energy differences between the two identical levels derived from two different line pairs, i.e., using the Ritz combination principle in the same way as in the previous articles [6, 7, 9]. For example, the energy difference between the levels 4 and 6 of Ga-like Nd^{29+} can be derived from the wavelength difference of different line pairs: (12.3473 nm and 14.3626 nm) and (17.9683 and 22.5806 nm). The first and second line pairs give rise to the energy differences 113640 (60) cm^{-1} and 113680 (40) cm^{-1} which is in very good agreement. This agreement validates the consistency of the present identifications. A similar analysis is also applicable to the levels 7 and 13 of Ge-like Nd^{28+}.

Following the methodology in the previous papers [6, 7], the energy levels of highly charged Nd ions derived from the present line identifications are summarized in Table 2 where the level energies and their uncertainties are listed in units of cm^{-1}. The uncertainties of the level energies are derived from the wavelength uncertainties of the corresponding lines listed in table 1. With regard to the level energies derived from multiple transitions by means of the Ritz combination principle, we took the square root of the sum of the squares of each energy uncertainty. Some of the levels have no connection to the ground level of that ion via the identified transitions listed in Table 1. In such a case, the level energy is evaluated by the connection to a reference level, the energy of which is derived from theoretical calculation. For example, the energy of level

Table 2: Energy levels of highly charged neodymium ions derived from the present line identifications. The column 'Energy' lists the level energies in cm^{-1}, and '+x' means that the energy of the reference level is taken from theoretical calculation. The last column lists the energy uncertainties derived from the wavelength uncertainties of the corresponding lines listed in table 1. 'RMBPT' and 'FAC' in the last column indicate the energies calculated by relativistic many body perturbation theory [49] and Flexible Atomic Code [26], respectively.

Ion	Conf.	State	Level#	Energy (cm^{-1})		Unc. (cm^{-1})
32+ [Ni]	$3d^{10}$	$(3d_+^6)_0$	1	0		0
32+ [Ni]	$3d^9 4p$	$((3d_-^3)_{3/2}, 4p_-)_1$	9	7512020		RMBPT
32+ [Ni]	$3d^9 4p$	$((3d_+^5)_{5/2}, 4p_+)_1$	12	7595030	+x	140
32+ [Ni]	$3d^9 4d$	$((3d_-^3)_{3/2}, 4d_-)_0$	35	8860960	+x	90
31+ [Cu]	4s	$(4s_+)_{1/2}$	1	0		0
31+ [Cu]	4p	$(4p_-)_{1/2}$	2	528880		20
31+ [Cu]	4p	$(4p_+)_{3/2}$	3	794240		40
31+ [Cu]	4d	$(4d_-)_{3/2}$	4	1642620		80
31+ [Cu]	4d	$(4d_+)_{5/2}$	5	1697070		70
31+ [Cu]	4f	$(4f_+)_{7/2}$	7	2616160*		90
30+ [Zn]	$4s^2$	$(4s_+^2)_0$	1	0		0
30+ [Zn]	4s4p	$(4s_+, 4p_-)_1$	3	496900		10
30+ [Zn]	4s4p	$(4s_+, 4p_+)_1$	5	829120		40
30+ [Zn]	$4p^2$	$(4p_-, 4p_+)_2$	8	1299990		120
30+ [Zn]	4s4d	$(4s_+, 4d_+)_2$	14	1752920		70
30+ [Zn]	4s4f	$(4s_+, 4f_+)_3$	30	2696410		90
29+ [Ga]	4p	$(4p_-)_{1/2}$	1	0		0
29+ [Ga]	4p	$(4p_+)_{3/2}$	2	253400		60
29+ [Ga]	$4s4p^2$	$(4s_+)_{1/2}$	3	507430*		10
29+ [Ga]	$4s4p^2$	$((4s_+, 4p_-)_0, 4p_+)_{3/2}$	4	696250		60
29+ [Ga]	$4s4p^2$	$((4s_+, 4p_-)_1, 4p_+)_{5/2}$	5	741140		60
29+ [Ga]	$4s4p^2$	$((4s_+, 4p_-)_1, 4p_+)_{3/2}$	6	809890		30
29+ [Ga]	$4s4p^2$	$((4s_+, 4p_-)_1, 4p_+)_{1/2}$	7	836600*		60
29+ [Ga]	$4s4p^2$	$(4s_+, (4p_+^2)_2)_{5/2}$	8	975500*		90
29+ [Ga]	$4s4p^2$	$(4s_+, (4p_+^2)_2)_{3/2}$	10	1089790*		50
29+ [Ga]	4d	$(4d_-)_{3/2}$	11	1172940		40
29+ [Ga]	4s4p4d	$((4s_+, 4p_-)_1, 4d_+)_{5/2}$	23	1735010*		40
28+ [Ge]	$4p^2$	$(4p_-^2)_0$	1	0		0
28+ [Ge]	$4p^2$	$(4p_-, 4p_+)_1$	2	218280		FAC
28+ [Ge]	$4p^2$	$(4p_-, 4p_+)_2$	3	244100		20
28+ [Ge]	$4p^2$	$(4p_+^2)_2$	4	482350		70
28+ [Ge]	$4s4p^3$	$(4s_+, 4p_+)_2$	6	720340	+x	20
28+ [Ge]	$4s4p^3$	$(4s_+, 4p_+)_1$	7	807080		20
28+ [Ge]	$4s4p^3$	$((4s_+, 4p_-)_0, (4p_+^2)_2)_2$	8	924910	+x	20
28+ [Ge]	$4s4p^3$	$((4s_+, 4p_-)_1, (4p_+^2)_2)_3$	9	973110		60
28+ [Ge]	4p4d	$(4p_-, 4d_-)_2$	11	1030750		50
28+ [Ge]	$4s4p^3$	$((4s_+, 4p_-)_1, (4p_+^2)_0)_1$	12	1044430	+x	40
28+ [Ge]	$4s4p^3$	$((4s_+, 4p_-)_1, (4p_+^2)_2)_1$	13	1087900		40

Table 2: (Continued.)

Ion	Conf.	State	Level#	Energy (cm^{-1})	Unc. (cm^{-1})
28+ [Ge]	4p4d	$(4p_-, 4d_-)_2$	14	1106620	170
28+ [Ge]	4p4d	$(4p_-, 4d_+)_3$	15	1176890*	70
28+ [Ge]	4p4d	$(4p_-, 4d_-)_1$	16	1185510	40
28+ [Ge]	4p4d	$(4p_+, 4d_-)_3$	23	1397180*	160
28+ [Ge]	$4s4p^24d$	$(4s_+, 4d_+)_2$	33	1732260*	30
27+ [As]	$4p^3$	$(4p_+)_{3/2}$	1	0	0
27+ [As]	$4p^3$	$(4p_-, (4p_+^2)_2)_{3/2}$	2	209840*	60
27+ [As]	$4s4p^4$	$(4s_+, (4p_+^2)_2)_{5/2}$	6	717530	60
27+ [As]	$4s4p^4$	$(4s_+, (4p_+^2)_2)_{3/2}$	7	790430*	30
27+ [As]	$4p^24d1$	$(4d_-)_{3/2}$	9	872110	50
27+ [As]	$4p^24d1$	$(4d_+)_{5/2}$	10	934680*	150
27+ [As]	$4p^24d1$	$((4p_-, 4p_+)_1, 4d_+)_{5/2}$	21	1150550*	130
27+ [As]	$4p^24d1$	$((4p_-, 4p_+)_1, 4d_+)_{3/2}$	22	1158370	40
27+ [As]	$4p^24d1$	$((4p_-, 4p_+)_2, 4d_+)_{3/2}$	25	1195830	70
27+ [As]	$4p^24d1$	$((4p_-, 4p_+)_2, 4d_+)_{5/2}$	28	1239150*	70
26+ [Se]	$4p^4$	$(4p_+^2)_2$	1	0	0
26+ [Se]	$4s4p^5$	$(4s_+, (4p_+^3)_{3/2})_2$	6	743010	30
26+ [Se]	$4s4p^5$	$(4s_+, (4p_+^3)_{3/2})_1$	7	790780*	40
26+ [Se]	$4p^34d1$	$(4p_+, 4d_-)_3$	10	854580	40
26+ [Se]	$4p^34d1$	$(4p_+, 4d_-)_1$	11	884390	20
26+ [Se]	$4p^34d1$	$(4p_+, 4d_+)_2$	13	928060	60
26+ [Se]	$4p^34d1$	$(4p_+, 4d_+)_3$	14	962630	60
26+ [Se]	$4p^34d1$	$((4p_-, (4p_+^2)_0)_{1/2}, 4d_+)_2$	31	1175460	120
26+ [Se]	$4p^34d1$	$((4p_-, (4p_+^2)_2)_{3/2}, 4d_-)_3$	32	1189040	110
25+ [Br]	$4p^5$	$(4p_+^3)_{3/2}$	1	0	0
25+ [Br]	$4p^44d$	$((4p_+^2)_2, 4d_+)_{5/2}$	14	972600	100
25+ [Br]	$4p^44d$	$((4p_-, (4p_+^3)_{3/2})_2\ 4d_-)_{5/2}$	27	1204490	40

* derived from blended line.

9 of Ni-like Nd^{32+} is taken from a calculation with relativistic many-body perturbation theory (RMBPT) [49] which would give more realistic level energies for Ni-like ions, and the energies of levels 12 and 35 are evaluated by the measured transitions connected to the level 9. Similarly, we used the present FAC calculation for the energy of level 2 of Ge-like Nd^{28+} as the RMBPT data are unavailable for Ge-like Nd ions at the present time. The level energies evaluated in this way are listed with "+x" in Table 2. Some of the energy levels can be determined by multiple pairs of the measured transitions. In this case, we chose one line pair which does not include blended lines. For example, the energy of level 2 of Ga-like Nd^{29+} can be derived from 4 different transition pairs, but three of them are relevant to blended lines. Therefore, we chose the unblended line pair (14.3626 nm and 22.5806 nm) to determine the energy of level 2.

5. Summary

We have identified 59 spectral lines of Ni-like to Br-like Nd ions in the 6 nm to 23 nm wavelength range using a series of accurate EUV spectra taken with the NIST EBIT for the electron beam energies in the range of 0.90 keV to 2.31 keV. The measured wavelengths for 9 lines of Ni-, Cu- and Zn-like ions are in excellent agreement with the previous observations. The remaining 50 lines have been newly assigned in this study. Similar studies of other lanthanide elements at the NIST EBIT facility and other EBITs would be helpful for further extension of the experimental data of EUV spectra from highly charged heavy ions in the future.

Acknowledgments

This work was partially supported by the NIST Measurement Science and Engineering (MSE) Research Grants (#70NANB18H282 and #70NANB19H024), the National Science Foundation (#1806494), and by NASA/GSFC (#80NSSC18K0234). One of the authors (CS) acknowledges financial support for his work at NIST by NIFS/NINS under Young Researchers Supporting Program (UFEX106), and by JSPS KAKENHI Grant (#15H03759).

References

[1] O'Sullivan G *et al* 2015 *Phys. Scr.* **90** 054002
[2] O'Sullivan G *et al* 2015 *J. Phys. B: At. Mol. Phys.* **48** 144025
[3] Sheil J *et al* 2017 *J. Phys. B: At. Mol. Phys.* **50** 065006
[4] Suzuki C, Higashiguchi T, Sasanuma A, Arai G, Fujii Y, Kondo Y, Dinh T -H, Koike F, Murakami I, O'Sullivan G 2017 *Nucl. Instrum. Methods Phys. Res. B* **408** 253
[5] Lokasani R *et al* 2018 *J. Phys. B: At. Mol. Phys.* **51** 215001
[6] Kilbane D, O'Sullivan G, Podpaly Y A, Gillaspy J D, Reader J and Ralchenko Yu 2014 *Eur. Phys. J. D* **68** 222
[7] Podpaly Y A, Gillaspy J D, Reader J and Ralchenko Yu 2015 *J. Phys. B: At. Mol. Phys.* **48** 025002
[8] Dipti, Silwal R, Dreiling J M, Sanders S C, Takacs E and Ralchenko Yu 2020 *J. Phys. B: At. Mol. Phys.* **53** 145002
[9] Kilbane D, O'Sullivan G, Gillaspy J D, Ralchenko Yu and Reader J 2012 *Phys. Rev.* A **86** 042503
[10] Ohashi H, Sakaue H A and Nakamura N 2013 *Phys. Scr.* **T156** 014013
[11] Gaigalas G, Kato D, Rynkun P, Radžiūtė L and Tanaka M 2019 *ApJS* **240** 29
[12] Reader J and Luther G 1980 *Phys. Rev. Lett.* **45** 609
[13] Reader J and Luther G 1981 *Phys. Scr.* **24** 732
[14] Acquista N and Reader J 1984 *J. Opt. Soc. Am.* B **1** 649
[15] Hinnov E, Beiersdorfer P, Bell R, Stevens J, Suckewer S, Goeler S von, Wouters A, Dietrich D, Gerassimenko M and Silver E 1987 *Phys. Rev.* A **35** 4876
[16] Seely J F, Feldman U, Wouters A W, Schwob J L and Suckewer S 1989 *Phys. Rev.* A **40** 5020
[17] Sugar J, Kaufman V, Baik D H, Kim Y-K and Rowan W L 1991 *J. Opt. Soc. Am.* B **8** 1795
[18] Sugar J, Kaufman V and Rowan W L 1991 *J. Opt. Soc. Am.* B **8** 2026
[19] Daido H, Ninomiya S, Takagi M, Kato Y and Koike F 1999 *J. Opt. Soc. Am.* B **16** 296
[20] Suzuki C, Koike F, Murakami I, Tamura N and Sudo S 2012 *J. Phys. B: At. Mol. Phys.* **45** 135002
[21] Suzuki C *et al* 2017 *Plasma Phys. Control. Fusion* **59** 014009

[22] Gillaspy J D 1997 *Phys. Scr.* **T71** 99
[23] Holland G E, Boyer C N, Seely J F, Tan J N, Pomeroy J M and Gillaspy J D 2005 *Rev. Sci. Instrum.* **76** 073304
[24] Blagojević B *et al* 2005 *Rev. Sci. Instrum.* **76** 083102
[25] Ralchenko Yu and Maron Y 2001 *J. Quant. Spectrosc. Radiat. Transfer* **71** 609
[26] Gu M F 2008 *Can. J. Phys.* **86** 675
[27] Dipti, Buechele S W, Gall A C, Sanders S, Szabo C I, Silwal R, Takacs E and Ralchenko Yu 2020 *J. Phys. B: At. Mol. Phys.* **53** 115701
[28] Gall A C, Dipti, Buechele S W, Sanders S, Szabo C I, Silwal R, Ralchenko Yu, Brickhouse N and Takacs E 2020 *J. Phys. B: At. Mol. Phys.* **53** 145004
[29] Nilsen J and Moreno J C 1995 *Opt. Lett.* **20** 1386
[30] Ivanova E P 2015 *Opt. Spectrosc.* **118** 506
[31] Scofield J H and MacGowan B J 1992 *Phys. Scr.* **46** 361
[32] Li Y, Nilsen J, Dunn J, Osterheld A L, Ryabtsev A and Churilov S 1998 *Phys. Rev.* A **58** R2668
[33] Suzuki C, Koike F, Murakami I, Tamura N and Sudo S 2018 *Atoms* **6** 24
[34] Goyal A, Khatri I, Aggarwal S, Singh A K and Mohan M 2016 *At. Data Nucl. Data Tables* **107** 406
[35] Seely J F, Brown C M and Feldman U 1989 *At. Data Nucl. Data Tables* **43** 145
[36] Biémont E 1988 *At. Data Nucl. Data Tables* **39** 157
[37] Blundell S A 1993 *Phys. Rev.* A **47** 1790
[38] Kim Y K, Baik D H, Indelicato P and Desclaux J P 1991 *Phys. Rev.* A **44** 148
[39] Biémont E 1989 *At. Data Nucl. Data Tables* **43** 163
[40] Brown C M, Seely J F, Kania D R, Hammel B A, Back C A, Lee R W, Bar-shalom A and Behring W E 1994 *At. Data Nucl. Data Tables* **58** 203
[41] Hao L H and Liu J J 2018 *J. Appl. Spectrosc.* **85** 730
[42] Safronova U I and Safronova M S 2010 *J. Phys. B: At. Mol. Phys.* **43** 074025
[43] Chen M H and Cheng K T 2010 *J. Phys. B: At. Mol. Phys.* **43** 074019
[44] Blundell S A, Johnson W R, Safronova M S and Safronova U I 2008 *Phys. Rev.* A **77** 032507
[45] Vilkas M J and Ishikawa Y 2005 *Phys. Rev.* A **72** 032512
[46] Hu F, Yang J, Wang C, Zhao X, Zang H, Jiang G and Hao L 2012 *At. Data Nucl. Data Tables* **98** 301
[47] El-Sayed F and Attia S M 2016 *J. Appl. Spectrosc.* **83** 126
[48] Wang K, Yang X, Chen Z B, Si R, Chen C Y, Yan J, Zhao X H and Dang W 2017 *At. Data Nucl. Data Tables* **117-118** 1
[49] Safronova U I, Safronova A S, Hamasha S M and Beiersdorfer P 2006 *At. Data Nucl. Data Tables* **92** 47